



ELSEVIER

Contents lists available at SciVerse ScienceDirect

Journal of Fluids and Structures

journal homepage: www.elsevier.com/locate/jfs

Tree-inspired piezoelectric energy harvesting

William B. Hobbs^a, David L. Hu^{a,b,*}^a School of Mechanical Engineering, Georgia Institute of Technology, Atlanta, GA 30332, USA^b School of Biology, Georgia Institute of Technology, Atlanta, GA 30332, USA

ARTICLE INFO

Article history:

Received 23 July 2010

Accepted 6 August 2011

Keywords:

Vortex induced vibrations

Piezoelectric energy harvesting

Tandem cylinders

ABSTRACT

We design and test micro-watt energy-harvesters inspired by tree trunks swaying in the wind. A uniform flow vibrates a linear array of four cylinders affixed to piezoelectric energy transducers. Particular attention is paid to measuring the energy generated as a function of cylinder spacing, flow speed, and relative position of the cylinder within the array. Peak power is generated using cylinder center-to-center spacings of 3.3 diameters and flow speeds in which the vortex shedding frequency is 1.6 times the natural frequency of the cylinders. Using these flow speeds and spacings, the power generated by downstream cylinders can exceed that of leading cylinders by more than an order of magnitude. We visualize the flow in this system by studying the behavior of a dynamically matched flowing soap film with imbedded styrofoam disks. Our qualitative visualizations suggest that peak energy harvesting occurs under conditions in which vortices have fully detached from the leading cylinder.

© 2011 Elsevier Ltd. All rights reserved.

1. Introduction

Energy harvesting is the process by which ambient energy is captured from external sources (thermal, wind, solar and hydrodynamic). One way to harvest energy is through the use of piezoelectricity, the ability of certain materials such as bone (Fukada and Yasuda, 1957), wood (Fukada, 1955) and ceramics to generate electric fields in response to mechanical strain. In this study, we investigate the feasibility of using biologically inspired kinetic sculptures to harvest energy by swaying in the wind. We examine primarily the use of ceramic piezoelectric transducers, but the principles we find may be applied to transducers composed of other materials.

While primarily used for sensing pressure, ceramic piezoelectric transducers have been recently implemented in several designs for fluid flow energy harvesting. They are envisioned for use in generating micro- and milli-watts for powering remote sensor networks and small-scale electronic devices. Some piezoelectrics replace electrical generators in conventional cam-driven rotating turbine designs (Priya et al., 2005). Other designs have been implemented to operate entirely differently from rotating designs. One example is the piezoelectric eel, an underwater sheet of piezoelectric polymer that oscillates in the wake of a bluff body (Taylor et al., 2001). The “oscillating blade” generator resembles a stalk of corn, in which a piezoelectric transducer connects a steel leaf spring to leaf-like ears (Schmidt, 1992).

Vortex-induced vibration is one of the primary mechanisms by which moving fluids cause objects to undergo oscillation, and is often capitalized upon in piezoelectric energy harvesting. The subject has a long history of experimental, theoretical and computational work, summarized in reviews by Bearman (1984), Williamson and Govardhan (2004), and

* Corresponding author at: School of Mechanical Engineering, Georgia Institute of Technology, 801 Ferst Drive, MRDC 1308, Atlanta, GA 30332-0405, USA. Tel.: +1 404 894 0573; fax: +1 404 894 8496.

E-mail address: hu@me.gatech.edu (D.L. Hu).

Blevins (1990), and more recently in Bearman (2011) and Sumner (2010). For a single cylinder in uniform flow, the periodic shedding of vortices will generate lateral pressure asymmetries on the cylinder. If the cylinder is elastic, vibrations transverse to the flow direction will also occur (Tanida et al., 1973; Zhou et al., 1999). A second cylinder downstream from the first will also vibrate due to vortices shed upstream (Allen and Henning, 2003; Gaydon and Rockwell, 1999; Lin et al., 2002; Mittal and Kumar, 2001, 2004; Mizushima and Suehiro, 2005), and under certain circumstances with larger amplitudes than that of the first cylinder (Huera-Huarte and Bearman, 2011). To and Lam (2007) investigated the behavior of a flexible cylinder placed upstream of a large stationary cylinder. Three and four cylinders have been studied in various arrangements, but the effect of cylinder vibration on flow structure is less frequently taken into account. Several investigators have studied triangular arrays of fixed non-vibrating cylinders (e.g., Lam and Cheung, 1988; Tatsuno et al., 1998). An array of cylinders arranged transverse to the flow has been studied for the purpose of underwater energy harvesting of the ocean's currents (Bernitsas et al., 2008). However, the energy generation behind multiple elastic cylinders arranged in a line received little attention. This is precisely the configuration for an orchard of trees (de Langre, 2008; Dupont and Brunet, 2008), and in our energy-harvesting device.

In this study, we present the design of a new piezoelectric device that uses tree-like swaying to harvest wind energy. The power output of our design is on the order of micro-watts, which on the same order of magnitude as other piezoelectric energy devices. This level of power is adequate for powering ultra-low power micro-controllers with sensing, recording, and wireless communication capabilities. In Section 2, we overview our device design and use this physical picture to conduct a dimensional analysis of our design in Section 3. In Section 4, we describe the methods used to collect energy data from our device and to dynamically match our system to a flowing soap film used for flow visualization. In Section 5, we present our experimental results, focusing on characterizing peak energy generation of our device over a range of device spacings and flow speeds. In Section 6, we discuss the efficiency of our device and provide guidelines for setting up the device for maximum power generation. In Section 7, we discuss the implications of our work and suggest directions for future research.

2. Device design considerations

A photograph of our device is shown in Fig. 1. The device consists of cylinders affixed to the ground via piezoelectric disks. The disk orientation permits cylinder tilting only in the cross-flow direction only, as shown in Fig. 2. In our early tests, we found that more degrees of freedom were unnecessary. For example, two degrees of freedom resulted in 95% of the vibration occurring in the transverse direction, in agreement with the results of Jauvtis and Williamson (2004).

Previous approaches for studying elastic cylinders have focused on increasing the amplitude of oscillation by optimizing the reduced damping as shown in the so-called “Griffin plots” (Khalak and Williamson, 1999). We stress that their analysis does

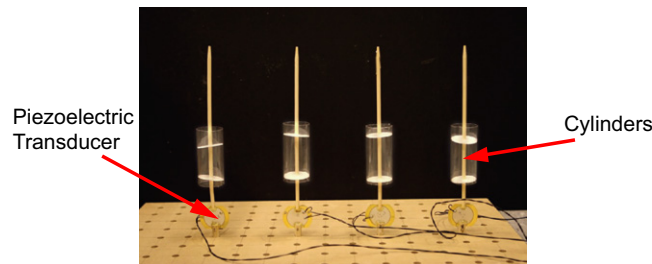


Fig. 1. Photograph of four piezoelectric devices in series.

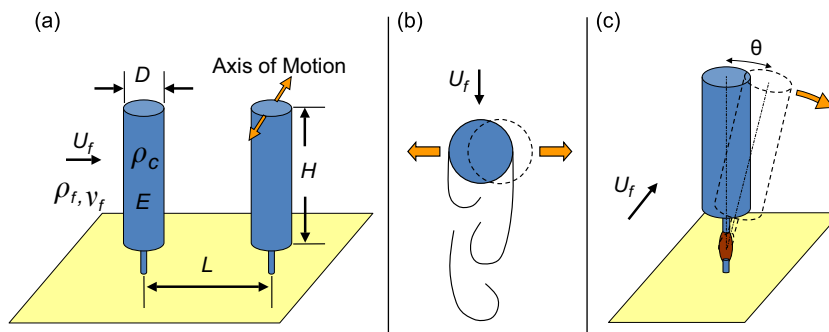


Fig. 2. Schematic diagrams illustrating the arrangement of energy-harvesting cylinders. (a) Side view of the cylinders, along with variables characterizing the properties of the flow and the cylinder. (b)–(c) Top and front views. Yellow arrows indicate the direction of cylinder vibration, which is transverse to the incoming flow. (For interpretation of the references to color in this figure legend, the reader is referred to the web version of this article.)

Table 1

Comparison of key parameters between the two-dimensional soap film system and the three-dimensional wind tunnel system.

Parameter	2-D System	3-D System
f_s/f_n	0.8–2.0	0.8–2.0
U (m/s)	1.1–2.8	1.8–4.3
Re	3550–8900	4100–9800
ρ_c/ρ_f	30	80
ζ	0.018 ± 0.005	0.072 ± 0.011

not consider the role of the mechanical damping, which in our case is equivalent to power production. While we do report damping in this study (see Table 1), we do not optimize with respect to it. Instead, we focus on maximizing power output with respect to cylinder spacing and flow speed. Efforts were also made to make the device's cross-section as thin as possible so that it could be implemented in large numbers while minimizing space. As shown in Fig. 1, we plan to implement our design in large numbers, which will enable us to take advantage of potential cooperative interactions, such as those observed in animal aggregations. In schools of fish, fish can minimize their swimming energy expended by harvesting vortex energy from fish upstream (Liao, 2007; Whittlesey et al., 2010). Similarly, we hope that an appropriate choice for the spacings of our devices will also augment energy harvesting.

3. Dimensional analysis

The physical picture of our system is shown in Fig. 2. We consider an in-line array of cylinders with a geometry described by cylinder diameter D , height H and center-to-center spacing L . The cylinders have material properties described by density ρ_c , elasticity E and dimensionless damping coefficient ζ . The fluid has density ρ_f , viscosity μ and far-field velocity U . Using dimensional analysis, we can write the power generated P , relative to other parameters, as

$$P = \rho_f U^3 D H \times g \left(\text{Re}, \frac{L}{D}, \frac{H}{D}, \frac{f_s}{f_n}, \frac{\rho_c}{\rho_f}, \zeta \right), \quad (1)$$

where $\rho_f U^3 D H$ is the rate of working of the fluid on the cylinder and the function g depends on Reynolds number $\text{Re} = UD/\nu$, dimensionless spacing L/D and cylinder height H/D , dimensionless shedding frequency f_s/f_n , mass ratio ρ_c/ρ_f and damping coefficient ζ . We now discuss the significance and magnitude of these dimensionless groups in turn. Their values are given in Table 1.

Over the velocities tested, the Reynolds number ranged from approximately $\text{Re} = 4000$ to 9000 indicating that viscosity effects were negligible. Cylinders were much heavier than the fluid (providing a mass parameter $\rho_c/\rho_f \approx 85$). We note that although the motion of the cylinder is rotational (see Fig. 2), the amplitude of motion is sufficiently small that we consider the motion to be effectively two dimensional rather than three dimensional.

We used cylinders with dimensionless height $H/D = 2.2$ and dimensionless spacing $L/D = 2-6$. Decreasing the dimensionless height will play a role in making the flow more fully three dimensional by accentuating tip effects (vortices shed over the top of the cylinder). We keep this height at an intermediate value in order to increase the similarity between the piezoelectric system and our two-dimensional soap film visualizations.

Finally, the dimensionless group f_s/f_n is the ratio of vortex shedding frequency, f_s , to the natural frequency, f_n , of the elastic cylinders. In particular, resonance of the cylinder corresponds to $f_s/f_n = 1$. In our experiments, the natural frequency f_n of our cylinders was found experimentally to be 11 Hz, and cylinders under flow conditions continued to vibrate at 11–12 Hz. Since we expect high energy generation to occur at resonance, we tuned the flow speed U so that $f_s/f_n = 0.8-2.0$.

To ease manufacturing, our devices consisted of rigid cylinders with an elastic hinge (the piezoelectric) at the base. For the sake of future workers, we also relate the group f_s/f_n to the intrinsic properties of an equivalent cylinder made of a single homogeneous material. We assume that elastic cylinders for our system shed at the same frequency as rigid fixed cylinders. For a single rigid cylinder in flow, the frequency, f_s , by which vortices are shed is given by the Strouhal number $S = f_s D/U$ (Blevins, 1990). As specified for a circular cross-section by Blevins (1990), the Strouhal number for a single cylinder is $S = 0.2$. Work by Igarashi (1986) would suggest that for fixed cylinders in tandem, a value of $S = 0.2$ is expected for flows with a Reynolds number below 10 000, with decreases to $S = 0.14$ during bistable behaviors. In our study, we will assume that oscillation of the cylinder has no impact on Strouhal number and use the value given by Blevins: $S = 0.2$.

Using the derivations of Van Eysden and Sader (2009), the resonant frequency for a circular beam in a fluid can be written according to the material properties of the beam and fluid:

$$f_n \sim \frac{D}{H^2} \left(\frac{E}{\rho_c} \right)^{1/2} \left(1 + \frac{\pi \rho_f}{4 \rho_c} \right)^{-1/2}. \quad (2)$$

Given that $\rho_f \ll \rho_c$, we can write f_s/f_n as

$$\frac{f_s}{f_n} \sim \frac{SU}{\sqrt{E/\rho_c}} \left(\frac{H}{D}\right)^2. \quad (3)$$

We do not explicitly use Eq. (3) in our methods. Instead, we predict f_s (using the appropriate Strouhal number) and we measure f_n directly with high-speed video, rather than inferring it through measurements of E . In the next section, we present our methods to measure peak power, as given in Eq. (1), specifically by characterizing the dependence of g on cylinder spacing and frequency ratio.

4. Methods

To design our devices and measure their performance, we used techniques from electrical engineering and fluid mechanics, which we discuss in turn.

4.1. Power measurements

We began by calibrating cylinder kinematic data (Fig. 2) with electrical measurements. Specifically, we used high-speed video to verify quantitatively that the angular velocity ω of the cylinders was proportional to voltage output V :

$$\omega = cV \quad (4)$$

where $\omega = d\theta/dt$ is the angular velocity. This was a logical relationship, as the voltage across a piezoelectric material is proportional to the rate of deformation of the material. Moreover, the deflection of our devices was less than $\theta = 6^\circ$, for which the small angle approximation is valid. The correlation constant $c \approx 0.4 \text{ (s V)}^{-1}$ was found by measuring the voltage across a $1 \text{ M}\Omega$ resistor while simultaneously measuring the displacement of the tip of the cylinder with calibrated high-speed video. The results of this testing are shown in Fig. 4, where the cylinder angle and angular velocity are plotted against the scaled voltage output of the piezoelectric transducer. The simple relation, Eq. (4), between voltage and angular velocity, greatly simplified interpretation of our results: it allowed us to characterize cylinder kinematics by simply recording voltage rather than high-speed video.

To verify that tilting of our cylinders was primarily in the cross-flow direction, we performed high-speed video of the device. We observed less than 1° of tilting in the stream-wise direction (compared to 6° of tilting in the cross-stream direction).

For all experiments, the voltage from each piezoelectric transducer was measured across a $1 \text{ M}\Omega$ resistance, using a sampling rate of 200 Hz using a PC with a multichannel data acquisition board running LabView™. The power output, P , for each device was calculated using the well-known relation $P = V^2/R$ where R is the resistance. Tests were carried out with a sampling duration of 60 s , and each test was then repeated 5 times to help insure the reliability of the data. The steady-state power for each cylinder was estimated by taking the root-mean-square (rms) power $P_{\text{rms}} = (\sum_t P^2(t))^{1/2}$ using 1200 total power measurements P at a series of time points t , with a sampling rate 200 Hz over a duration of 60 s . Note that we use the rms power because this is the standard for electronics and power generation. We found that tests of such a long duration (compared to the time-scale of cylinder motion $1/10 \text{ s}$) were necessary to obtain repeatable values for cylinder power. For example, Fig. 5 shows a plot of the 60-s moving average of the P_{rms} of the four devices during a single test. The high variation in voltage can be clearly seen in the first 5–10 s of the data.

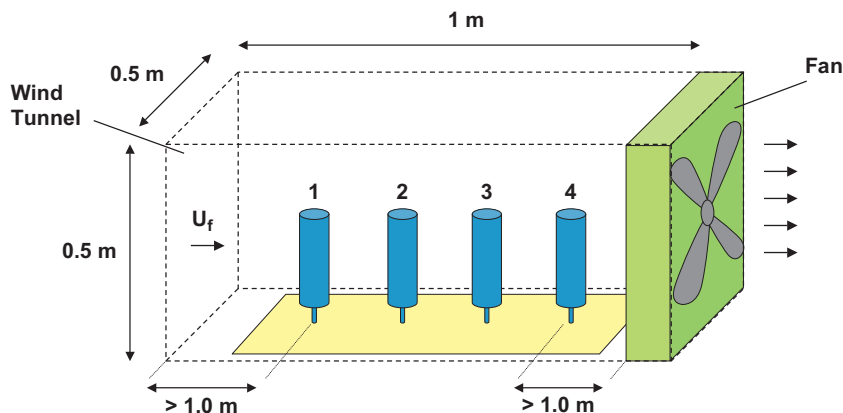


Fig. 3. Schematic diagram of the wind tunnel used for testing. Cylinders are numbered 1 (leading cylinder) to 4 (most downstream cylinder). Air is drawn through the tunnel, from the left to the right, by a box fan. To minimize edge effects, the first and last device in the series were positioned at least 0.1 m from the ends of the 1 m long tunnel.

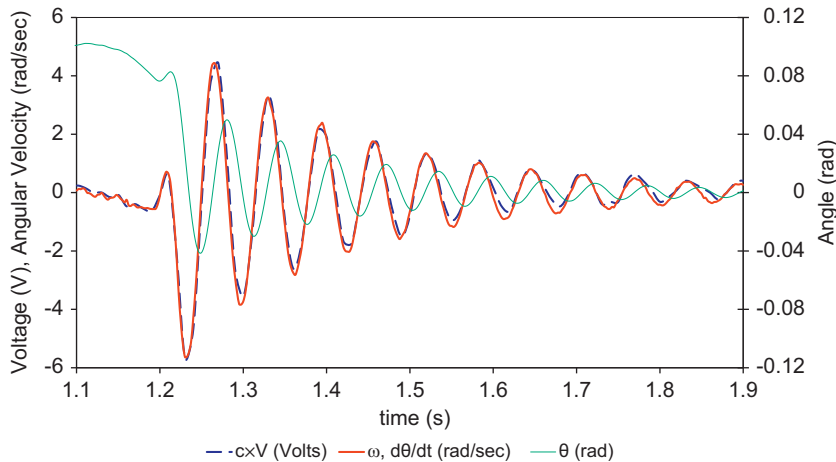


Fig. 4. Motion and scaled voltage of an oscillating piezoelectric device. Angle and angular velocity were measured with high-speed video, and voltage was simultaneously measured with an oscilloscope to obtain the relationship, c , between angular velocity and voltage.

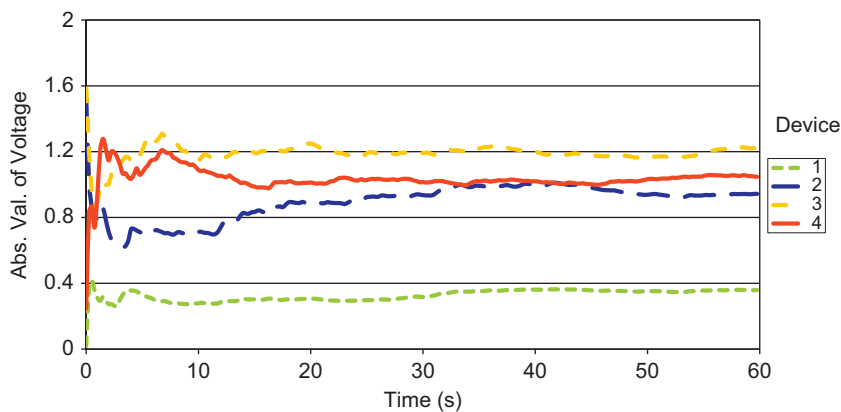


Fig. 5. Moving average of absolute value of voltage output from each of the four devices. Note that the long-duration drifts in power output necessitates testing for at least 60 s in duration.

We used the measurements of individual cylinder power P'_{rms} to estimate the relative performance of the cylinder within the array. The total power generated in the array is defined as $P_{tot} = P_1 + P_2 + P_3 + P_4$ where each cylinder has rms power P_i . This power was then non-dimensionalized using the scaling, $P' = P/(\rho U^3 DH)$.

4.2. Device construction

The cylinder walls were made of polyethylene storage tubes (McMaster-Carr Supply Company, 35 mm inner diameter, 0.4 mm thick, length of $H=78$ mm). Tubes were attached to a bamboo rod (a 4.7 mm diameter, 22 cm long) using a pair of styrofoam spacers. A piezoelectric transducer was epoxied to the bamboo rod by a slit ~ 1 cm deep cut into the base of the rod. Piezoelectric transducers consisted of disks intended for use as audio buzzers. They were composed of two ceramic layers sandwiching a 42 mm diameter brass plate between the layers (PUI Audio, part number AB4113B). On the base of the transducer, a peg was epoxied on to enable arrangement of several devices on a wooden pegboard (with center-to-center holes spaced 1.5 in apart). The two layers of the transducer were connected in series, and wires were then run from each to a breadboard, from which voltage readings were taken. To tune each of the devices, such that its resonant frequency was 11 Hz, common metal paper clips were attached to the top of the bamboo rods, and slid up and down the rod to change the rotational moment of inertia.

A schematic of the arrangement of four cylinders used in our tests is shown in Figs. 1 and 3. The pegboard base allowed the arrangement of the devices to be adjusted. Cylinders were slid up and down the bamboo stick to adjust mass distribution to tune the device to the appropriate natural frequency. Fig. 3 demonstrates the experimental setup placed in a wind tunnel. The piezoelectric transducers and cylinders are labeled 1 (the leading cylinder) through 4 (the most downstream cylinder). To compensate for small differences in the mechanical to electrical conversion efficiency of each device, as they were made by hand, the power output of each device was normalized. This was done by rotating the

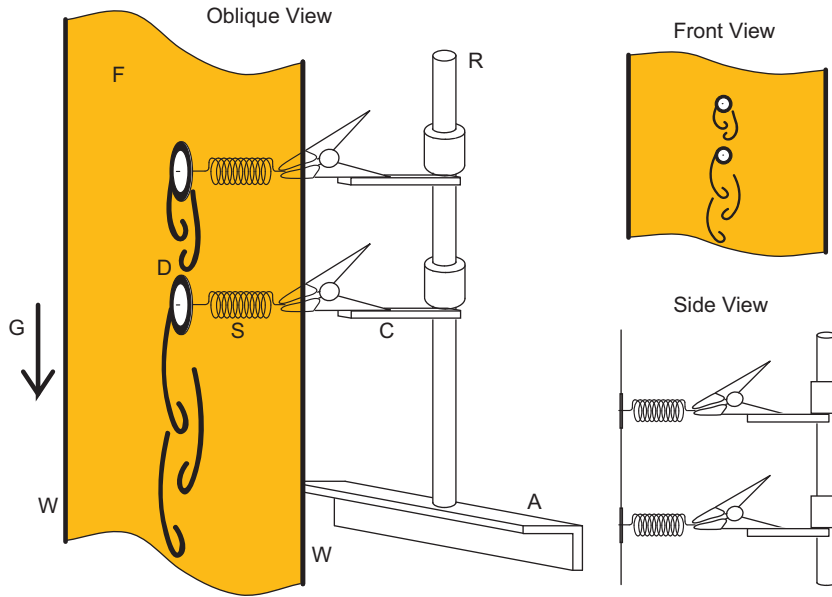


Fig. 6. Schematic diagram (oblique, front and side views) of our soap film apparatus. Disks (D) in the soap film (F) are suspended from linear springs (S) behind the film. The film flows top to bottom, pulled by gravity (G). The clamps are vertically adjustable along a rod (R), which is fixed to an angled aluminum support (A). The wires (W) that support the film are also shown.

devices through each position, while keeping the other positions occupied, and measuring the average power output. Scaling factors (of 1.26, 1.0, 1.08 and 1.30 for devices 1–4) were applied such that each device, on average, would generate the same amount of power given the same conditions. These scaling factors were then applied to each individual device's output for the remainder of our testing.

Flow velocity in the wind tunnel was controlled by a combination of built-in speed controls on the fan and a 120 VAC Variac™ variable transformer. Calibration of the system for flow speed was provided by velocity measurements using a hand held anemometer, insuring that variation in velocity was less than 5% over the area that the piezoelectric devices would be placed.

The damping ratio ζ was calculated for the piezoelectric devices as well as the soap film system by measuring the logarithmic decrement. Devices in each system were manually deflected and released (i.e., a step input) and the oscillating response was recorded. By measuring the decreasing motion over at least four oscillations, the damping ratio was estimated, as given in Table 1. We also verified using incremental deflection tests that the springs were indeed linear in the range of flow speeds considered.

To better understand the relation between vortex shedding and power output, a three-cylinder system was visualized in a dynamically matched two-dimensional flowing soap film (Fig. 6). Detailed descriptions of using a soap film water tunnel are given in Beizaie and Gharib (1997) and Ristroph and Zhang (2008). We suspended styrofoam disks (diameter $D=12.5$ mm) in the soap film using springs. Spring stiffness was chosen to provide dynamic similarity with the piezoelectric system. Dimensionless parameters for our wind tunnel and soap film tests are given in Table 1. Tests were run at two different spacings, $L/D=2$ and 5, and two different flow speeds, which provided frequency ratios of $f_s/f_n=0.5$ and 1.5.

5. Results

5.1. Peak power in the array

We characterized the power parameter space by collecting 96 piezoelectric power measurements (consisting of four devices across four different spacings and six flow speeds). Fig. 7 shows a contour plot of combined dimensionless power. Moving to the right on the contour plot corresponds to increased wind speed; moving upward corresponds to increased spacing.

Clearly, Fig. 7 shows a global peak in power at spacings L/D near 3.3 and frequency ratios f_s/f_n near 1.6. We draw insight on the position of this peak using flow visualization of representative points (a–d) in Fig. 7. Images of the corresponding flows are shown in Fig. 8. There are clear visible differences between the flow structures corresponding to low power output (a–b) and high power output (c–d). Specifically, in the high-power conditions (c–d), vortices are detached from the leading and second cylinder. This causes the second and third cylinder to be buffeted by the vortices from the arising Kármán (1963) vortex streets. Conversely, in the low-power conditions (a–b), the leading cylinder is trailed by regions of

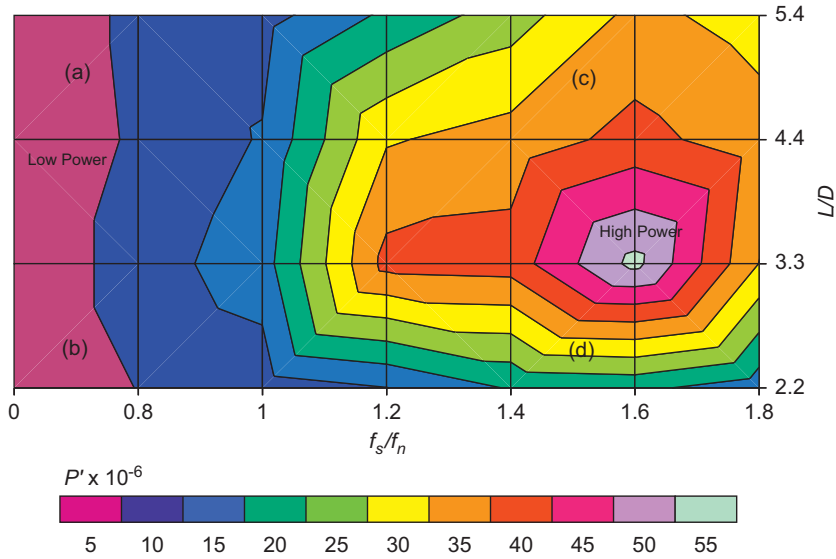


Fig. 7. Contour plot of the dimensionless power, $P'_1 + P'_2 + P'_3 + P'_4$, for all four devices as a function of frequency ratio f_s/f_n and spacing L/D . Regions of low power (on the left) and high power (on the right) are labelled. In these regions are also labelled as four characteristic points (a–d) for which flow visualizations were conducted in a soap film (Fig. 8).

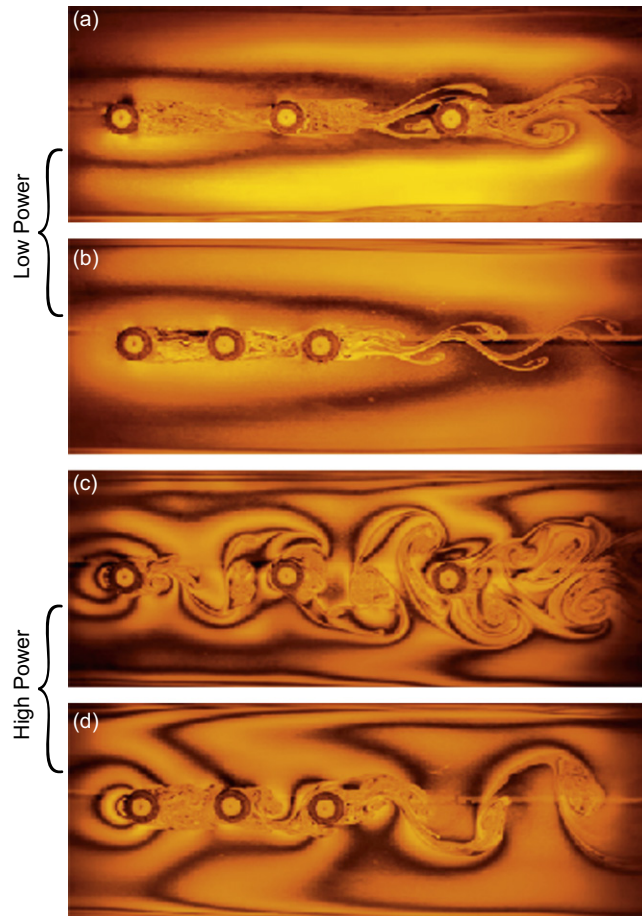


Fig. 8. Soap film visualizations of flow around three spring-loaded cylinders (1.25 cm diameter). Flow is from left to right and conditions have been dynamically matched to the piezoelectric system, whose power output is given in Fig. 7. Specifically, (a–b) denote low power generation and (c–d) high power generation.

recirculation. Clearly, vortices do not fully detach from the cylinders until after the most downstream cylinder. We conclude that for generating high power, cylinder spacing and flow speeds should be sufficiently large for Kármán vortex wakes to fully develop. This result is consistent with the work of Zdravkovich and others, who have shown that the lift of a trailing cylinder is strongly influenced by the alternating, discrete vortices in the wake of an upstream cylinder (Liang et al., 2009; Zdravkovich, 1987).

As shown by our flow visualizations, peak power is associated with a fully developed Kármán vortex street. Conversely, at low wind speeds (Fig. 8a–b), Kármán vortex streets are only generated by the most downstream cylinder. The remaining cylinders are surrounded by stagnant and recirculating regions, causing minimal cylinder vibration and a minimum in power for the array: here $P'_{\text{tot}} \approx 5 \times 10^{-6}$ is at a global minimum. At such low wind speeds, changes in spacing (as shown in Fig. 8a) do not appreciably develop the vortex street. Correspondingly, power appears to be relatively invariant of spacing.

We expect dimensional power to be dependent on wind-speed, as shown by the U^3 scaling in Eq. (1). Surprisingly, there appear to be further nonlinear effects, as dimensionless power also increases dramatically with flow speed, as shown by the peak in power at high wind speeds on the right-hand side of Fig. 7. Thus, at high wind speeds, dimensionless power is $P'_{\text{tot}} \approx 55 \times 10^{-6}$, or 10 times higher than the dimensionless power at low wind speeds.

In order to further understand why there is such a dramatic increase in power for certain spacings and wind speeds, we estimate how relative power changes at different positions in the array. First, we average across all spacings (across horizontal lines in Fig. 7) to find power due to changes in flow speed.

5.2. Relative power in the array for changes in wind speeds

Fig. 9 shows the relative power of cylinders 1–4 over a range of flow speeds. We observe highly nonlinear behavior. First, clearly, the leading cylinder generates negligible power ($P' = 10^{-6}$) for all wind speeds. This reinforces the notion, as suggested by the soap film visualizations (Fig. 8), that a Kármán vortex street is necessary for power generation in this system. Apparently, a Kármán street following a cylinder is insufficient; instead, the cylinders should be buffeted by an incoming wake. The low power from the leading cylinder suggests to future workers that the leading cylinder might be replaced with a dummy to reduce production costs.

At low flow speeds (so that $f_s/f_n = 0.8$ – 1.0), all cylinders are at comparable power production (all within $P' = 4 \times 10^{-6}$). At intermediate flow speeds (near resonance, $f_s/f_n = 1.2$ to 1.4), the third cylinder from the leading edge has a peak power over an order of magnitude higher than the leading cylinder. Over the highest flow speeds ($f_s/f_n > 1.4$), the peak-producing cylinder is instead the most downstream one.

In Fig. 9, we observed how relative power in the array changed with flow speed. Results were averaged across spacings. How does relative power change with cylinder spacing? To answer this question, examine horizontal lines in Fig. 7. Specifically, by averaging power across all flow speeds, we can show how spacing influences power generation.

5.3. Relative power in the array for changes in spacing

Fig. 10 shows the changes in relative power down the array over a range of spacings. This plot was generated by averaging data across wind speeds. Similarly to Fig. 9, we observe that the leading cylinder exhibits the lowest power output. Moreover, the third and fourth cylinders exhibit the greatest power generation. A substantial increase in power

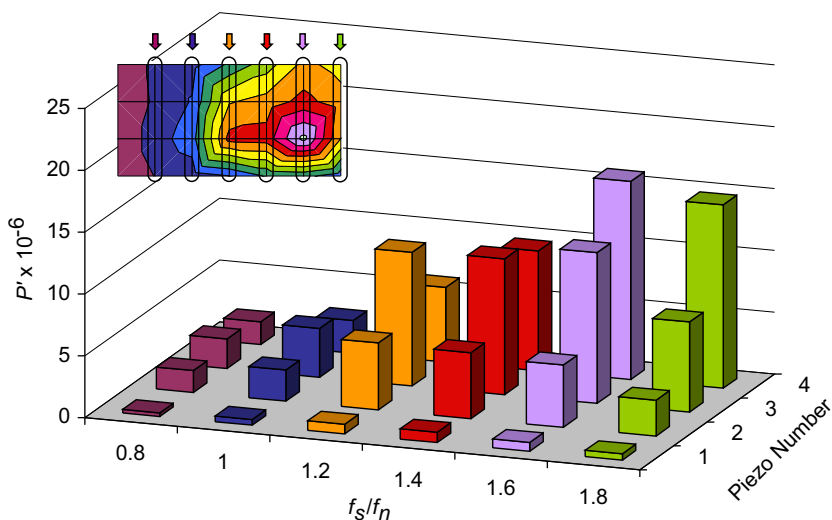


Fig. 9. Dimensionless power for each piezoelectric device, averaged across spacings. Inset, corresponding to Fig. 7, highlights the groups of data that were averaged to obtain each row of values. Piezos are numbered 1–4, according to Fig. 3.

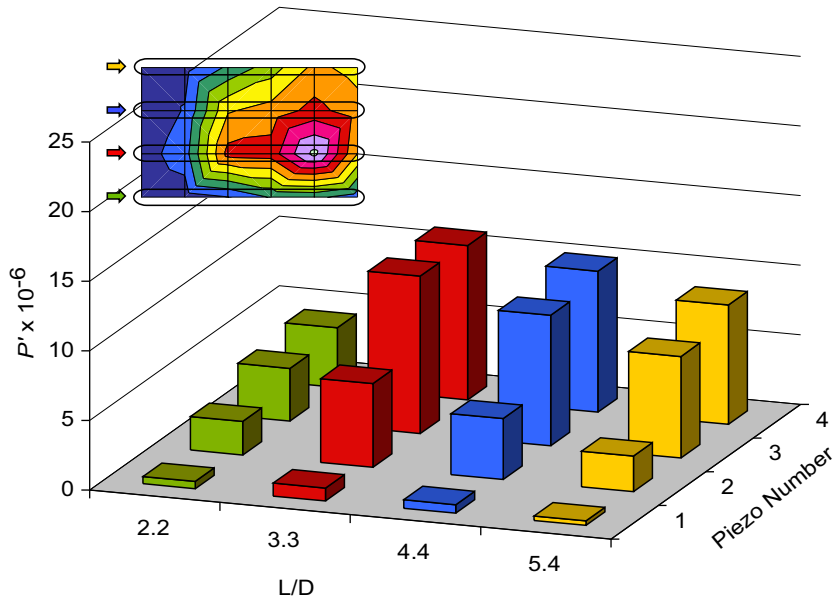


Fig. 10. Dimensionless power for each piezoelectric device, averaged across frequency ratios. Inset, corresponding to Fig. 7, highlights the groups of data that were averaged to obtain each row of values.

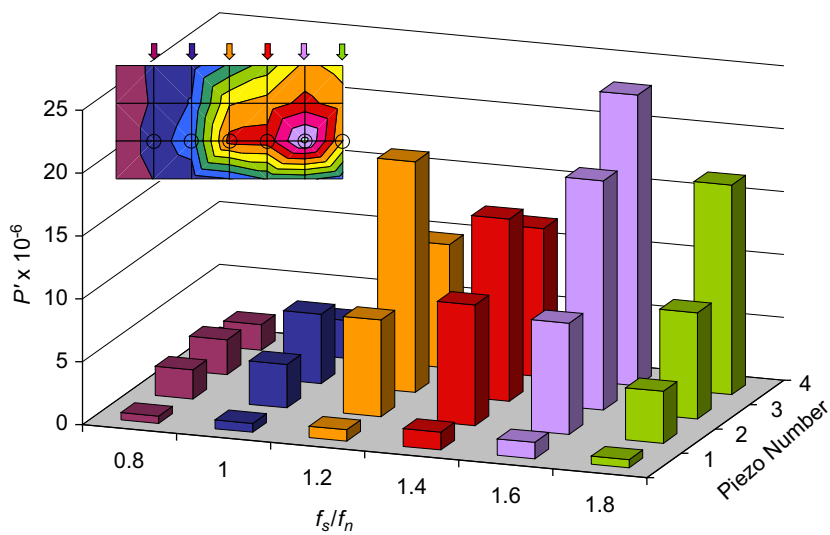


Fig. 11. Dimensionless power for each piezoelectric device, with spacing fixed at $L/D=3.3$.

(from $P' = 3 \times 10^{-6}$ to $P' = 10 \times 10^{-6}$) in the third cylinder occurs as spacing increases from 2.2 to 3.3. Clearly, a spacing of 3.3 ± 1 seems to be the best for energy harvesting. To further examine how the power changes close to a spacing of 3.3 would require further tests. Since a spacing of 3.3 seems optimal, we next examine how wind speed affects power production at this particular spacing.

5.4. Relative power for changes in wind speed, given a fixed spacing $L/D=3.3$

Fig. 11 shows the relative power in the array for changes in wind speed. The spacing is fixed at $L/D=3.3$. Without averaging across spacings, the effects shown in Fig. 9 are further amplified, showing peak power occurring at the 3rd and 4th cylinders. Peak power is produced at wind speeds such that $f_s/f_n = 1.6$. Higher wind speeds ($f_s/f_n > 1.6$) cause the power in all the cylinders to decrease.

6. Efficiency and power output

In this section, we report the efficiency and maximum power generated by our device. We first note that these values depend explicitly on the quality of the piezoelectric we used. Efficiency would very likely increase if our transducer was replaced with a higher quality piezoelectric bimorph, such as the one used by Priya et al. (2005).

Power output from each of our devices ranged from 1 to 5 μW for the wind conditions tested. This value is low in comparison to a device built by Priya (2005), which is smaller than our device, yet produces 3 orders of magnitude more power. We suspect that the primary reason for this large discrepancy is the differences in quality of the piezoelectric used. Nevertheless, milli-watts and micro-watts are typical values for piezoelectric power generation. These values are in part so much lower than conventional wind turbines because of their small size necessitated by the high cost of the piezoelectric materials.

As shown by other workers in piezoelectrics, power magnitude is not the only metric motivating their implementation. Piezoelectrics have been shown to be useful for mobile or low-power applications such as remote sensing, wireless data transmission or LED lighting. We found that we were able to light a single ultra low-power LED under the wind conditions tested. We also found that four of our devices could provide power to low power micro-controllers capable of logging and transmitting sensor data, such as the MSP430 Line (Texas Instruments, 2009).

For the flows considered ($U = 1.8\text{--}4.3$ m/s) and the cross-sectional area of the device $DH = 28$ cm², the incoming power is $\rho U^3 DH = 0.016\text{--}0.22$ W. Given the Betz efficiency of 59%, a wind turbine with the same cross-sectional area of our cylinders would produce at most 0.01–0.1 W of power. Although wind turbines generate significantly more power, our device still has several advantages. For example, our device may require less maintenance than a wind turbine as it has no rotating parts and no gearbox. This simplicity also provides potential for the device to be scaled down in size more easily than that of a wind turbine.

A portion of the energy of deformation of the piezoelectric material is harvested. Thus, the kinetic energy KE associated with the cylinder's vibrating can give us an upper bound for the deformation energy. This $\text{KE} = \frac{1}{2}I\omega^2$ where the moment of inertia $I = MH^2/12 \approx 30$ g cm² using a cylinder mass of $M = 10$ g. Given an amplitude of vibration ($\theta = 6^\circ = \pi/30$ rad) and frequency ($f = 1/10$ cycles s⁻¹), the angular velocity is $\omega = 1$ rad s⁻¹. Thus, the $\text{KE} = 3 \times 10^{-6}$ J, which represents an upper bound of the energy that can be harvested per cycle. The maximum power that can be harvested is $P_{\text{max}} = \text{KE} \times f$, which may be written as

$$P_{\text{max}} = \frac{1}{96}\pi\rho_c D^2 H^3 \theta f^3, \quad (5)$$

where we have used $M = \frac{1}{4}\rho_c \pi D^2 H$ as the mass of our device. Using the length and time-scales of our device, the maximum possible power generated is $P_{\text{max}} = 10^{-5}$ W, or 10 μW , with a maximum power harvested per unit area of 0.3 μW per square cm. The scaling in Eq. (5) provides several possible avenues for improving energy generation. For example, a more compliant piezoelectric material would increase the amplitude of bending θ , but may decrease the frequency f . The easiest way to increase the energy generated is to build a larger device. For example, a device the size of a large oak tree (2 orders of magnitude larger in all dimensions) would, by virtue of Eqs. (2) and (5), increase P_{max} by four orders of magnitude, thus increasing the power to the order of 1 W.

How does the power generated by each cylinder compare to this upper bound? The dimensionless power P' is the ratio of the device's power to the rate of working of the fluid over the cylinder's area. Therefore P' also denotes the efficiency of our device. We found that leading cylinder in the flow has an efficiency of one millionth ($P' = 1 \times 10^{-6}$). The low efficiency is due largely because of the low mass of the device, which stores very little kinetic energy. The corresponding power per unit area is $10^{-7}\text{--}10^{-8}$ W per square cm.

As we saw from our measurements, a single cylinder in isolation would make a poor energy-harvester. Instead, the 3rd and 4th cylinders in the array tend to generate the majority of the array's power (each roughly generating 25 times the power of the leading cylinder). Consequently, an array of four cylinders (in which the last two generate the most power) has an efficiency of $P' = 55 \times 10^{-6}$, as shown in Fig. 7. Thus, the addition of more cylinders behind the leading one tends to increase the efficiency of the group of devices, as the cross-sectional area remains fixed.

7. Discussion

The flow past a group of cylinders is a canonical example of a simple situation that can lead to complex behavior. This physical picture has motivated much work, such as investigations of the flow through cities, plant wind vibrations, heat transfer of tube-banks, as well as fundamental fluid mechanics. Here, we have used this canonical system as the blueprint for a novel piezoelectric device that uses vortex-induced vibrations to harvest wind energy. We found that such a device necessarily relies upon cooperative effects for peak energy harvesting. Specifically, we found that a piezoelectric cylinder works poorly in isolation. However, when grouped together, the flows generated by upstream cylinders can dramatically increase the power generated by cylinders downstream.

We demonstrated the cooperative effect of our piezoelectric tests using two independent experiments. First, we used wind tunnel tests to measure the power produced by the array of cylinders as well as the relative power produced down the array. Next, we conducted flow visualizations in a dynamically matched soap film. Our results suggest that high power was associated with full development of Kármán vortex streets after the leading cylinder.

We found striking increase in power generated by simple changes in cylinder arrangement. For example, dimensionless power was found to increase by up to 300% at cylinder spacings of $L/D=3.3$ compared to that of other spacings. This result is consistent with the work of Zdravkovich and Pridden (1977), which found that cylinders with a spacing below $L/D=3$ would fail to shed vortices.

We were also able to investigate how our device would fare under different wind conditions. We showed that there is an optimal wind speed for power production. Finding the highest power at flow speeds associated with $f_s/f_n = 1.6$ was unusual, as we expected non-dimensional power to peak at or near resonance ($f_s/f_n = 1$). One explanation for this revolves around our assumptions regarding vortex shedding frequency. First, we assumed that the vortex shedding frequency for the oscillating cylinders would be the same as that of stationary cylinders, thus not accounting for effects of frequency lock-in. Second, we assumed that vortex shedding would only occur in the horizontal plane, which may not have been true, given the fairly low aspect ratio of the cylinders. These combined factors may have resulted in peak power to occur at $f_s/f_n = 1.6$ rather than 1, but more study is necessary to understand this phenomenon.

Future generations of our device will likely use more than four cylinders, and more work is needed to understand the limitations of adding devices. We found that for intermediate wind speeds, power increased up to the third device, and then decreased at the fourth. However, for higher wind speeds, power increased through the fourth device. The causes for these two behaviors may be resolved by adding more devices, until the relationship between power and position in the array is better understood. We speculate that the explanation for these behaviors lies in a balance between the flow changes caused by and the energy removed by upstream devices. Imaging of the vorticity on the flow and its time-dependence would provide a much-needed understanding of the behaviors observed.

Typical wind-harvesting devices, such as wind turbines, are meant to be used in isolation and in steady flow. Turbines are rarely grouped in-line, as the resulting vortex shedding and unsteady flows cause stress to turbine blades. By studying one- and two-dimensional arrays of devices, we hope future workers can devote more attention to energy harvesting that relies upon unsteady effects. We hope that we have drawn attention to the complex dynamics and potential advantages of designing energy-harvesters to be arranged in an orchard-like fashion.

Appendix A. Supplementary material

Supplementary data associated with this article can be found in the online version of [10.1016/j.jfluidstructs.2011.08.005](https://doi.org/10.1016/j.jfluidstructs.2011.08.005).

References

- Allen, D., Henning, D., 2003. Vortex-induced vibration current tank tests of two equal-diameter cylinders in tandem. *Journal of Fluids and Structures* 17, 767–781.
- Bearman, P., 1984. Vortex shedding from oscillating bluff bodies. *Annual Review of Fluid Mechanics* 16, 195–222.
- Bearman, P., 2011. Circular cylinder wakes and vortex-induced vibrations. *Journal of Fluids and Structures* 27, 648–658.
- Beizaie, M., Gharib, M., 1997. Fundamentals of a liquid (soap) film tunnel. *Experiments in Fluids* 23, 130–140.
- Bernitsas, M., Raghavan, K., Ben-Simon, Y., Garcia, E., et al., 2008. Vivace (vortex induced vibration aquatic clean energy): a new concept in generation of clean and renewable energy from fluid flow. *Journal of Offshore Mechanics and Arctic Engineering* 130, 041101.
- Blevins, R.D., 1990. *Flow-induced Vibration*, second ed. Van Nostrand Reinhold, New York.
- Dupont, S., Brunet, Y., 2008. Impact of forest edge shape on tree stability: a large-eddy simulation study. *Forestry* 81, 299–315.
- Fukada, E., 1955. Piezoelectricity of wood. *Journal of the Physical Society of Japan* 10, 97–103.
- Fukada, E., Yasuda, I., 1957. On the piezoelectric effect of bone. *Journal of the Physical Society of Japan* 12, 1158–1162.
- Gaydon, M., Rockwell, D., 1999. Vortices incident upon an oscillating cylinder: flow structure and loading. *Journal of Fluids and Structures* 13, 709–722.
- Huera-Huarte, F., Bearman, P., 2011. Vortex and wake-induced vibrations of a tandem arrangement of two flexible circular cylinders with near wake interference. *Journal of Fluids and Structures* 27, 193–211.
- Igarashi, T., 1986. Characteristics of the flow around four circular cylinders arranged in line. *Bulletin of the JSME* 29, 751–757.
- Jauvtis, N., Williamson, C.H.K., 2004. The effect of two degrees of freedom on vortex-induced vibration at low mass and damping. *Journal of Fluid Mechanics* 509, 23–62.
- Kármán, T., 1963. *Aerodynamics*. McGraw-Hill Education.
- Khalak, A., Williamson, C., 1999. Motions, forces and mode transitions in vortex-induced vibrations at low mass-damping. *Journal of Fluids and Structures* 13, 813–851.
- Lam, K., Cheung, W., 1988. Phenomena of vortex shedding and flow interference of three cylinders in different equilateral arrangements. *Journal of Fluid Mechanics* 196, 1–26.
- de Langre, E., 2008. Effects of wind on plants. *Annual Review of Fluid Mechanics* 40, 141–168.
- Liang, C., Papadakis, G., Luo, X., 2009. Effect of tube spacing on the vortex shedding characteristics of laminar flow past an inline tube array: a numerical study. *Computers & Fluids* 38, 950–964.
- Liao, J., 2007. A review of fish swimming mechanics and behaviour in altered flows. *Philosophical Transactions of the Royal Society B: Biological Sciences* 362, 1973–1993.
- Lin, J.C., Yang, Y., Rockwell, D., 2002. Flow past two cylinders in tandem: instantaneous and averaged flow structure. *Journal of Fluids and Structures* 16, 1059–1071.
- Mittal, S., Kumar, V., 2001. Flow-induced oscillations of two cylinders in tandem and staggered arrangements. *Journal of Fluids and Structures* 15, 717–736.
- Mittal, S., Kumar, V., 2004. Vortex induced vibrations of a pair of cylinders at Reynolds number 1000. *International Journal of Computational Fluid Dynamics* 18, 601–614.
- Mizushima, J., Suehiro, N., 2005. Instability and transition of flow past two tandem circular cylinders. *Physics of Fluids* 17, 104107.
- Priya, S., 2005. Modeling of electric energy harvesting using piezoelectric windmill. *Applied Physics Letters* 87, 184101.
- Priya, S., Chen, C.T., Fye, D., Zahnd, J., 2005. Piezoelectric windmill: a novel solution to remote sensing. *Japanese Journal of Applied Physics: Part 2—Letters & Express Letters* 44, L104–L107.
- Ristroph, L., Zhang, J., 2008. Anomalous hydrodynamic drafting of interacting flapping flags. *Physical Review Letters* 101, 194502.

- Schmidt, V., 1992. Piezoelectric energy conversion in windmills. In: IEEE 1992 Ultrasonics Symposium Proceedings, vol. 2, pp. 897–904.
- Sumner, D., 2010. Two circular cylinders in cross-flow: a review. *Journal of Fluids and Structures* 26, 849–899.
- Tanida, Y., Okajima, A., Watanabe, Y., 1973. Stability of a circular-cylinder oscillating in uniform-flow or in a wake. *Journal of Fluid Mechanics* 61, 769–784.
- Tatsuno, M., Amamoto, H., Ishi-i, K., 1998. Effects of interference among three equidistantly arranged cylinders in a uniform flow. *Fluid Dynamics Research* 22, 297–315.
- Taylor, G.W., Burns, J.R., Kammann, S.M., Powers, W.B., Welsh, T.R., 2001. The energy harvesting eel: a small subsurface ocean/river power generator. *IEEE Journal of Oceanic Engineering* 26, 539–547.
- Texas Instruments, Inc., 2009. eZ430-Chronos Development Tool User's Guide, SLAU292.
- To, A., Lam, K., 2007. Flow-induced vibration of a flexibly mounted circular cylinder in the proximity of a larger cylinder downstream. *Journal of Fluids and Structures* 23, 523–528.
- Van Eysden, C., Sader, J., 2009. Resonant frequencies of a rectangular cantilever beam immersed in a fluid. *Journal of Applied Physics* 100, 114916.
- Whittlesey, R., Liska, S., Dabiri, J., 2010. Fish schooling as a basis for vertical axis wind turbine farm design. *Bioinspiration and Biomimetics* 5, 033005.
- Williamson, C.H.K., Govardhan, R., 2004. Vortex-induced vibrations. *Annual Review of Fluid Mechanics* 36, 413–455.
- Zdravkovich, M., 1987. The effects of interference between circular cylinders in cross flow. *Journal of Fluids and Structures* 1, 239–261.
- Zdravkovich, M.M., Pridden, D.L., 1977. Interference between 2 circular-cylinders—series of unexpected discontinuities. *Journal of Industrial Aerodynamics* 2, 255–270.
- Zhou, C.Y., So, R.M.C., Lam, K., 1999. Vortex-induced vibrations of an elastic circular cylinder. *Journal of Fluids and Structures* 13, 165–189.